2

SAINT PETERSBURG STATE UNIVERSITY STUDIES
IN EARTH SCIENCES

Anna S. Pakhomova

Crystal Chemistry of Natural and Synthetic Titanium and Molybdenum Oxocompounds

Saint Petersburg | 2013

The series Saint Petersburg State University Studies in Earth Sciences presents final results of research carried out in postgraduate geological programs at St. Petersburg State University. Most of this research is here presented after publication in leading scientific journals.

The supervisors of these works are well-known scholars of St. Petersburg State University and invited foreign researchers. The material of each book has been considered by a permanent editorial board as well as a special international commission comprised of well-known Russian and international experts in their respective fields of study.

Printed in Russia by St. Petersburg University Press
11/21 6th Line, St. Petersburg, 199004

ISSN 2308-6602
ISBN 978-5-288-05468-6

ABSTRACT

Crystal chemistry of molybdates and titanates is of special interest due to the appearance of these compounds in the nuclear fuel cycle. In the present study, several synthetic and natural molybdates and titanates were investigated by means of X-ray diffraction single-crystal structure analysis. Five novel alkali molybdates were synthesized and structurally characterised: β-$Cs_2Mo_4O_{13}$, $Cs_3(Mo_2O_7)Br$, $(emim)_3K(Mo_8O_{26})$, $(emim)_3Rb(Mo_8O_{26})$ and $(emim)_2Cs_2(Mo_8O_{26})$ (emim = 1-ethyl-3-methylimidazolium). The crystal structures of murataite-3C and -8C, members of the pyrochlore-murataite polysomatic series, have been solved. Their investigation provided unambiguous evidence for the modular nature of the series and explained crystallization sequence of murataite matrices from the crystal-chemical point of view. The structure of laachite, $(Ca,Mn)_2(Zr,Mn)_2Nb_2TiFeO_{14}$, a new mineral from the Laach See, Germany, was found to be monoclinic analogue of zirconolite-3*O*.

Supervisor Prof. Dr. Sergey V. Krivovichev
Department of Crystallography
Faculty of Geology
Saint-Petersburg State University, Russia

Opponents

Prof. Dr. Anatoly N. Zaitsev (Chairman)
Department of Mineralogy
Faculty of Geology
Saint-Petersburg State University, Russia

Prof. Dr. Vladimir G. Krivovichev
Department of Mineralogy
Faculty of Geology
Saint-Petersburg State University, Russia

Prof. Dr. Igor V. Pekov
Department of Mineralogy
Faculty of Geology
Moscow State University, Russia

Prof. Dr. Stanislav K. Filatov
Department of Crystallography
Faculty of Geology
Saint-Petersburg State University, Russia

Prof. Dr. Giovanni Ferraris
Department of Mineralogy and Petrology
University of Turin, Italy

Prof. Dr. Ronald Miletich-Pawliczek
Institute of Mineralogy and Crystallography
Faculty of Geosciences, Geography and Astronomy
University of Vienna, Austria

Prof. Dr. Olga V. Yakubovich
Department of Crystallography and Crystal Chemistry
Faculty of Geology
Moscow State University, Russia

ACKNOWLEGDEMENTS

There are no proper words either in Russian or English language to express all my gratitude to my supervisor Sergey V. Krivovichev. I am thankful to him for opening doors to the world of crystallography and attentive guidance inside it. I appreciate a lot his kind attitude, understanding and help with scientific problems as well as with life deals. I hope one day I will be able to do something worthy in return.

I would like to acknowledge all my colleagues from the Department of Crystallography of Saint-Petersburg University. I am particularly grateful to Daria Spiridonova who guided me during my first steps of the scientific work. I would like to express my great appreciation to Moscow colleagues for collaboration: Sergey V. Yudintsev (Institute of Geology of Ore deposites, Petrograghy, Mineralogy and Geochemistry), Sergey V. Stefanovsky (MosNPO Radon) and Nikita V. Chukanov (Institute of Problems of Chemical Physics). My grateful thanks are extended to Victor N. Yakovenchuk from the Kola Science Center of the Russian Academy of Sciences.

I wish to thank professor Thomas Armbruster and all Mineralogical Crystallography group from Bern University where I was lucky to work for 6 months during my PhD study. I highly appreciate the new experience and knowledge I got there.

Finally, I wish to thank my family and friends who always were with me. This work could not be done without their constant care and support.

Financial support was provided through the Federal Target Program "Scientific and Educational Professional Community of Innovative Russia" (contract no. 16.740.11.0490), the Russian Foundation for Basic Research (project no. 09-08-12000), and the St. Petersburg State University (grant no. 3.37.84.2011). X-ray diffraction studies were partially done in the X-ray Diffraction Resource Centre of St.Petersburg State University.

LIST OF FIGURES

LIST OF TABLES

CONTENTS

LIST OF INCLUDED ARTICLES

PI Pakhomova A. S., Krivovichev S. V. Tricaesium dimolybdate(VI) bromide. Acta Crystallographica. 2009, E65, i87.

PII Pakhomova A. S., Krivovichev S. V. Ionothermal synthesis and characterization of alkali metal polyoxometallates: Structural trends in the $(emim)_m[A_n(Mo_8O_{26})]$ (emim=1-ethyl-3-methylimidazolium; m=2,3; n=1,2; A=K, Rb, Cs) group of compounds. Inorganic Chemistry Communications. 2010, 13, 1463–1465.

PIII Pakhomova A. S., Spiridonova D. V., Krivovichev S. V. Crystal structure of β-$Cs_2Mo_4O_{13}$. Radiokhimiya. 2011, 53, 4, 304–306. [Radiochemistry (Engl. Transl.), 2011, 53, 4, 358–360].

PIV Laverov N. P., Urusov V. S., Krivovichev S. V., Pakhomova A. S., Stefanovsky S. V., Yudintsev S. V. Modular nature of the polysomatic pyrochlore-murataite series. Geologiya Rudnykh Mestorozhdenii. 2011, 53, 4, 307-329. [Geology of Ore Deposits (Engl. Transl.), 2011, 53, 273–294].

PV Pakhomova A. S., Krivovichev S. V., Yudintsev S. V., Stefanovsky S. V. Synthetic murataite-3C, a complex form for long-term immobilization of nuclear waste: crystal structure and its comparison with natural analogues. Zeitschrift fur Kristallographie. 2013, 223, 151–156.

OTHER PUBLICATIONS

AI Pakhomova A. S., Krivovichev S. V. Synthesis and crystal structure of new compound $Cs_2Mo_4O_{13}$. Volume of Abstracts of the International Scientific Conference "Fedorov Session 2008". Russia, Saint-Petersburg, 2008, p. 200–201. [in Russian]

AII Pakhomova A. S., Krivovichev S. V. Synthesis and crystal structure of new compound $Cs_2Mo_4O_{13}$. Abstracts of the III Russian Radiochemistry and Nuclear Technology School. Russia, Ozersk, 2008, p. 15–17. [in Russian]

AIII Pakhomova A. S., Krivovichev S. V. Synthesis and crystal structure of new compound $Cs_3(Mo_2O_7)Br$. II All-Russian Youth Conference "Minerals: Structure, Properties, Methods of Research". Russia, Miass, 2010, p. 290–291. [in Russian]

AIV Pakhomova A. S., Krivovichev S. V. Crystal chemistry of cesium molybdates. International Conference "Minerals as advanced materials II". Russia, Kirovsk, 2010, Book of Abstracts, p. 76–77.

AV Pakhomova A. S., Krivovichev S. V. Crystal chemistry of cesium molybdates. International Scientific Conference "Fedorov Session 2010". Russia, Saint-Petersburg, 2010, Abstr., p. 121–122.

AVI Pakhomova A. S., Krivovichev S. V. Ionothermal synthesis and characterization of alkalimetal polyoxometallates: Structural trends in the $(emim)_m[A_n(Mo_8O_{26})]$ (emim=1-ethyl-3-methylimidazolium; m=2,3; n=1,2; A=K, Rb, Cs) group of compounds). Abstracts of the 26th European Crystallographic Meeting. Acta Crystallographica. 2010, A66, s189.

AVII Pakhomova A. S., Krivovichev S. V. Ionothermal synthesis and characterization of alkali metal polyoxometallates: Structural trends in the $(emim)_m[A_n(Mo_8O_{26})]$ (emim=1-ethyl-3-methylimidazolium; m=2,3; n=1,2; A=K, Rb, Cs) group of compounds). Abstracts of the Xth Young Scientist Conference "Actual problems of inorganic chemistry: nanomaterials and human health". Russia, Zvenigorod, 2010, p. 43. [in Russian]

AVIII Krivovichev S. V., Urusov V. S., Yudintsev S. V., Pakhomova A. S., Stefanovsky S. V. Modular structures with cubic symmetry: polysomatic series pyrochlore-murataite. Abstracts of the VI National Crystal-chemical Conference. Russia, Suzdal, 2011, p. 55–56. [in Russian]

AIX Pakhomova A. S., Krivovichev S. V., Stefanovsky S. V., Yudintsev S. V. Natural murataite and its synthetic analogue murataite-3C: a comparison. Book of abstracts of XVII International Conference "Crystal Chemistry, X-ray Diffraction and Spectroscopy of Minerals". Russia, Saint-Petersburg, 2011, p. 104–105.

AX Pakhomova A. S., Krivovichev S. V., Stefanovsky S. V., Yudintsev S. V. Structural investigations of synthetic analogues of murataite. Book of abstracts of the XXII Congress and General Assembly of the International Union of Crystallography. Acta Crystallographica. 2011, A67, C573–C574.

AXI Pakhomova A. S., Krivovichev S. V., Stefanovsky S. V., Yudintsev S. V. Solution of crystal structures of murataite-3C and -8C — members of polysomatic series pyrochlore-murataite. Abstracts of the International Scientific Conference "Fedorov Session 2012". Russia, Saint-Petersburg, 2012, p. 446–447.

AXII Pakhomova A. S., Krivovichev S. V., Stefanovsky S. V., Yudintsev S. V. Solution of crystal structures of murataite-3C and -8C — members of polysomatic series pyrochlore-murataite. Abstracts of the Conference «Laue-100. X-ray structural investigations". Russia, Nigny Novgorod, 2012, p. 50–52. [in Russian]

AXIII Pakhomova A. S., Krivovichev S. V., Stefanovsky S. V., Yudintsev S. V. Structural investigations of synthetic members of pyrochlore-murataite polysomatic series. Abstract book of 28th European Crystallography Meeting. Acta Crystallographica. 2013, A69, s438.

AXIV Pakhomova A. S., Krivovichev S. V., Chukanov N. V. Crystal structure of laachite, a new zirconolite-related mineral from the Eifel volcanic region, Germany. Volume of abstracts of the 2nd International Conference "Clays, Clay Minerals and Layered Materials". Russia, Saint-Petersburg, 2013, p. 42.

1 INTRODUCTION

Problems associated with the use of nuclear energy are of particular interest from both scientific and public points of view. According to the data presented by the IAEA (International Atomic Energetic Agency), nuclear plants produce about 16% of the world energy (Energy…, 2011). In developed countries, portion of nuclear energy in overall energy balance exceeds the mean value of 50% and reach 74% in France, 51% in Belgium, 28% in Germany, 29% in Japan, 20% in USA and 17% in Russia. The activity of nuclear power plants inevitably leads to the formation of radioactive waste of high risk for the environment. Liquid high-level waste (HLW) that has complicated chemical and radioisotope composition (fuel elements (isotopes of U), transuranic actinides, fission products, components of fuel membranes, the reagents for the excretion of plutonium and uranium) is of special attention. Treatment of the HLW is highly sophisticated and is one of the most actual scientific problems of nuclear industry at the present time. In this perspective, molybdates and titanates were found to be compounds of particular interest.

Interest to *molybdates* is caused by the fact that oxidation of HLW results in formation of crystalline molybdate compounds and their crystal chemical studies are necessary for investigations and modeling the processes accompanying the decay of unstable uranium isotopes and their release into the environment. Molybdates have repeatedly been found in spent nuclear fuel. One ton of uranium fuel extracted from PWR (Pressurized water reactor) was reported to contain about 3.35 kg of Mo (Choppin *et al.*, 2001). Mo atoms are chemically active and tend to form alkali molybdates that due to the color were called a "yellow formation". Short *et al.* (2004) exemplified that yellow formation has a strong influence on the effectiveness of borosilicate glasses used for the SNF immobilization. In liquid state, these compounds cause corrosion of crucibles made from the Inconel alloys in vitrification-waste plants, whereas in solid state they can be water soluble and increase the degree of radionuclides leaching.

Interest in potassium, rubidium and cesium molybdates as compounds directly related to the nuclear fuel cycle induced detailed studies of their thermodynamic properties, phase diagrams and structural characteristics (Cordfunke, Konings, 1990; Ishii,

Mizuno, 1996; Minato *et al*., 1997). According to the literature, there are 23 potassium, rubidium and cesium molybdates known to the date. The first part of the thesis is devoted to the synthesis and structural characterization of alkali-metal-containing molybdates with different chemical compositions.

In contrast to molybdates, *titanates* do not form in the nuclear wastes, but instead are of special interest as promising materials for the radioactive waste immobilization. Isolation of the HLW through its incorporation into stable materials and their disposal in geological repositories is now considered as the most perspective approach in radioactive waste disposal. Among the most enduring proposals is that of the Synroc matrices that consist mainly of synthetic titanate analogues of zirconolite, pyrochlore, hollandite, rutile, perovskite, and murataite (Ringwood, 1985). From the viewpoint of the present study, the most interesting compounds are those with zirconolite- and murataite-pyrochlore-type structures.

Zirconolite. According to the modern classification (Bayliss *et al*., 1989) there are five mineral species in the zirconolite group: zirconolite; zirconolite -3T; zirconolite -2M; zirconolite -3O; zirkelite. Crystal chemical formula of these minerals can be presented as $(M1)_2^{VIII}(M2)_2^{VII}(M3)_3^{VI}(M4)^{IV,V}O_{14}$. End-member formula is $Ca_2^{VIII}Zr_2^{VII}Ti_3^{VI}Ti^{V}O_{14}$ and the idealized one is $CaZrTi_2O_7$. Zirconolites-3O, 3T и 2M are orthorhombic, trigonal and monoclinic polytypes of zirconolite, respectively.

Synthetic analogues of zirconolite form the basis of the Synroc matrices developed in 1980s by the group of Australian geochemists (Ringwood, 1985). In Synroc formulations, zirconolite is largely responsible for the immobilization of uranium and tetravalent actinides and to a lesser extent — for the immobilization of rare earths and trivalent actinides. About 25 % of UO_2 and ThO_2 can be incorporated into the zirconolite crystal structure. The U^{4+} cation is largely accommodated into the Zr site and to a lesser extent in the Ca site. In contrast, larger Th^{4+} ions are strongly partitioned into the Ca site, and is very reluctant to enter the Zr site. The compositional variety of natural and synthetic zirconolites demonstrates that the structure can accommodate a wide range of cation substitutions. This capacity is explained by the presence of five distinct cation sites suitable for a wide variety of species with diverse ionic charges and radii. As a consequence, zirconolite significantly contributes to the capacity of the Synroc formulations to accommodate high-level waste-stream of various compositions.

Murataite. Within last decade, titanate matrices composed of synthetic analogues of murataite were considered as perspective for the HLW immobilization. Natural murataite is a rare mineral discovered in alkaline pegmatites of the St. Peters Dome area, Colorado, U.S. (Adams *et al.*, 1974), and later found in the Baikal region in Russia (Portnov *et al*., 1981). Chemically murataite is titanate of heavy rare earth elements, zinc, sodium and iron. The crystal structure of murataite was determined by Ercit and Hawthorne (1995) as cubic, space group *F*-43*m*, a = 14.886 Å, Z = 4. The ideal and simplified formula of natural murataite can be written as $^{[8]}R_6{}^{[6]}M1_{12}{}^{[5]}M2_4{}^{[4]}TX_{43}$, where R = Y, HREE, Na, Ca, Mn, *M1* = Ti, Nb, Na, *M2* = Zn, Fe, Ti, Na, T = Zn, Si and X = O, F, OH.

Synthetic analogue of murataite was first identified in a titanate ceramic with the HLW imitators produced at the Savannah River nuclear plant in the U.S. (Morgan, Ry-

erson, 1982). Murataite investigations were intensified after its discovery in the Synroc matrix with the HLW wastes from the PO Mayak, a radiochemical facility for production and reprocessing of nuclear fuel in Russian Federation. (Laverov *et al*., 1997). Aside from zirconolite, hollandite, perovskite and rutile, that are typical constituents of Synroc, minor content of murataite was found. Five volume percent of this phase accumulated about 40% of the total uranium present in the sample, which led to detailed investigations of chemistry and properties of murataite and, in particular, of its chemical durability and radiation resistance (Laverov et al., $1998_{1\text{-}2}$, 1999, 2001, 2003, 2006; Lian *et al*., 2005; Stefanovsky *et al*., 2007; Yudintsev *et al*., 2007).

Transmission electron microscopy studies allowed to identify synthetic varieties of murataite with the 3×3×3, 5×5×5, 7×7×7 and 8×8×8 fluorite cubic supercells referred as murataite-3C, -5C, -7C and -8C phases, respectively. Urusov *et al.* (2005, 2007) put forward a proposal that synthetic murataites can be considered as members of murataite-pyrochlore polysomatic series built up from 2-dimensional (2D) structural modules. According to this proposal, synthetic varieties of murataite were considered as composed of two types of layered modules representing the parent murataite (*Mu-3)* and pyrochlore (*Pyr*) structures. Structure of murataite-5C was described as built from one *Mu-3* and one *Pyr* modules, whereas the structure of murataite-8C as based upon alternating two *Mu-3* and one *Pyr* modules. Structural investigations of murataite-5C (Krivovichev *et al.,* 2010) confirmed the modular nature of the polysomatic series. However, it was found that the structural modules are not two-dimensional layers, but zero-dimensional blocks. The structure of murataite-5C (sp. gr. *F*-43*m*, *a* = 24.564(7) Å) was found to be based upon cubic pyrochlore clusters with the diameter of *ca.* 1.5 nm arranged in a 3D chessboard-like fashion. They are linked by additional octahedra with formation of octahedral subframework. Non-octahedral cations form a murataite-like metal-oxide substructure. In the structure of *Mu*-5, the subframework of linked pyrochlore clusters and the murataite-like subframework units communicate by sharing those corners of TiO_6 octahedra, which are not involved in the subframework constructions.

Present thesis: goals, methods, overview. This work contains results of structural investigations of alkali metal molybdates and synthetic and natural titanates. It can be subdivided into three parts:

1. Synthesis and crystal chemical study of new alkali metal molybdates;
2. Crystal chemical study of synthetic modifications murataite-3C and -8C;
3. Structural investigations of laachite — a new zirconolite-type mineral.

In Section 2, we provide brief overview of the results obtained; detailed description of the experimental and theoretical achievements can be found in the original papers appended at the end of the thesis.

2 BRIEF DESCRIPTION OF RESULTS

This work contains results of synthetic and structural studies of novel molybdates and titanates. Crystallographic data and experimental parameters for the structures of the phases studied are listed in Table 1.

Table 1. Crystallographic data and refinement parameters for $Cs_2Mo_4O_{13}$ (**1**), $Cs_3(Mo_2O_7)Br$ (**2**), $(emim)_3K(Mo_8O_{26})$ (**3**), $(emim)_3Rb(Mo_8O_{26})$ (**4**) и $(emim)_2Cs_2(Mo_8O_{26})$ (**5**), murataite-3C (**6**), murataite-8C (**7**) and laachite (**8**)

	1	**2**	**3**	**4**	**5**	**6**	**7**	**8**
a (Å)	8.655(5)	6.3993(5)	9.5939(10)	10.9824(7)	8.2073(11)	14.676(15)	39.105(12)	7.3119(5)
b (Å)	8.396(5)	6.3993(5)	10.0236(11)	11.9599(7)	21.7847(26)	14.676(15)	39.105(12)	14.1790(10)
c (Å)	11.541(4)	16.9870(15)	11.9277(12)	16.5152(10)	10.6232(15)	14.676(15)	39.105(12)	10.1700(7)
α (°)	117.841(8)	90	111.133(8)	96.391(5)	90	90	90	90
β (°)	60.069(28)	90	110.867(8)	92.918(5)	110.243(11)	90	90	90.072(2)
γ (°)	109.761(5)	120	90.777(8)	103.465(5)	90	90	90	90
V (Å)	636.6(6)	584.71(8)	986.36(57)	2089.87(32)	1782.04(77)	3161.31(57)	59799.40(318)	1054.38(1)
Sp.gr.	*P*-1	$P6_3/mmc$	*P*-1	*P*-1	$P2_1/n$	*F*-43*m*	*F*-43*m*	*C*2/*c*
μ (cm^{-1})	38.95	14.77	26.60	35.69	48.30	10.604	26.32	15.089
λ (Å)	0.71073	0.71073	0.71073	0.71073	0.71073	0.71073	0.71073	0.71073
Total reflections	2218	5224	17777	20121	12706	13265	166610	11123
Unique reflections	2218	344	5328	10414	3774	761	12926	2319
Unique reflections $\|F_o\| \geq 4\sigma_F$	1644	338	4444	6901	3328	598	3706	1974
R_1	0.053	0.025	0.039	0.044	0.056	0.0630	0.1556	0.031
wR_2	0.159	0.062	0.092	0.092	0.123	0.1902	0.3476	0.076
S	1.049	1.180	1.082	0.872	1.080	1.057	1.172	1.087

2.1 Crystal chemical studies of alkali metal molybdates

2.1.1 Synthesis and crystal structure of β-$Cs_2Mo_4O_{13}$

Needle-like transparent crystals of the β-polymorph of cesium tetramolybdate $Cs_2Mo_4O_{13}$ (**Fig. 1a**) were obtained by hydrothermal reaction of lindgrenite $Cu_3(MoO_4)_2(OH)_2$ with aqueous solution of $CsNO_3$. The structure was solved from X-ray diffraction data collected by means of a STOE IPDS II diffractometer equipped with an Image plate area detector. The structure was solved by direct methods and refined to $R_1 = 0.053$. The SHELXL program package was used for all structural calculations (Sheldrick, 2008).

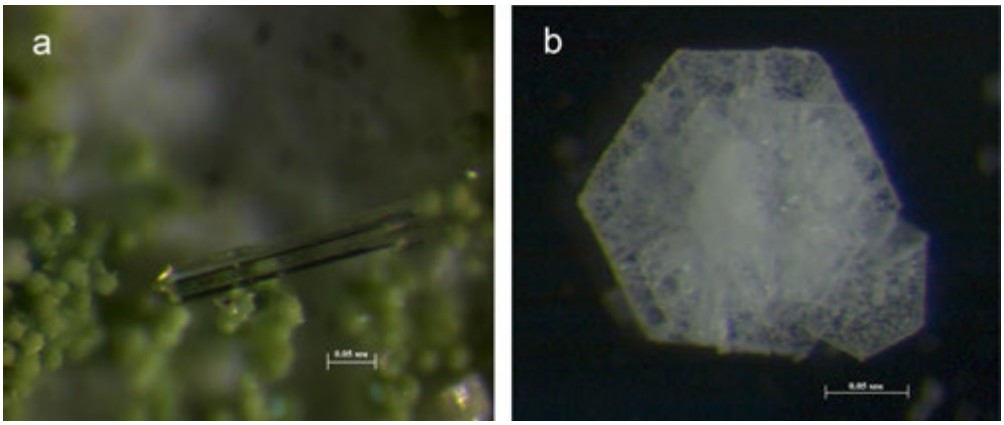

Fig. 1. a) Needle-like transparent crystal of β-$Cs_2Mo_4O_{13}$; b) hexagonal plate crystals of compound $Cs_3(Mo_2O_7)Br$.

β-$Cs_2Mo_4O_{13}$ is isostructural to the K and Rb tetramolybdates (Gatehouse, Leverett, 1971). There are four crystallography independent Mo sites coordinated by six O atoms each with the formation of distorted $[MoO_6]^{6-}$ octahedra. Eight octahedra share common edges to form octamolybdate complexes, which are further linked by sharing edges of peripheral octahedra so that zig-zag chains form running parallel to the *b* axis. Detailed description of crystal structure and experimental details can be found in paper PIII (see Included Articles).

2.1.2 Synthesis and crystal structure of $Cs_3(Mo_2O_7)Br$

Crystals of $Cs_3(Mo_2O_7)Br$ were prepared by the reaction of $CsNO_3$ (0.192 g), MoO_3 (0.146 g) and the ionic-liquid salt 1-ethyl-3-methylimidazolium bromide, [emim]Br (0.451 g) at 180°C for 3 days in a Teflon-lined steel autoclave with an interval volume of 20 ml. Transparent hexagonal plate crystals of $Cs_3(Mo_2O_7)Br$ were found (**Fig. 1b**). The structure was solved by direct methods from X-ray diffraction data collected by means of a STOE IPDS II Image Plate diffractometer. The structure was solved by direct methods and refined to $R_1 = 0.025$.

The structure of $Cs_3(Mo_2O_7)Br$ contains one symmetrically independent Mo^{6+} cation that is tetrahedrally coordinated by four O atoms. Two $(MoO_4)^{2-}$ tetrahedra share common O2 atom to form a $[Mo_2O_7]^{2-}$ dimer. The structure contains two symmetrically independent Cs positions. Cs1 is coordinated by nine O atoms and one Br atom, whereas Cs2 is coordinated by six O atoms and three Br atoms. The dimers $[Mo_2O_7]^{2-}$ are linked by Cs2 and Br atoms to form sheets parallel to (001). The three-dimensional connectivity of the structure is provided by Cs1 atoms located in the interlayer space.

$Cs_3(Mo_2O_7)Br$ is isostructural to previously studied $K_3(Mo_2O_7)Br$ (Becher, Fenske, 1978). In other dimolybdates, the $[Mo_2O_7]^{2-}$ dimers usually display Mo-O-Mo valence angles ranging from 141.4° ($Ce_2(MoO_4)_2(Mo_2O_7)$, Fallon, Gatehouse, 1982) to 160.6° ($Mg_2Mo_2O_7$, Stadnicka *et al.*, 1977). Detailed description of crystal structure and experimental details can be found in paper PI (see Included Articles).

2.1.3 Synthesis and crystal structure of K, Rb and Cs octamolybdates

Three new compounds, $(emim)_3K(Mo_8O_{26})$ (**1**), $(emim)_3Rb(Mo_8O_{26})$ (**2**) and $(emim)_2Cs_2(Mo_8O_{26})$ (**3**) were synthesized by ionothemal method with using 1-ethyl-3-methylimidazolium bromide ([emim]Br) as a solvent. X-ray diffraction data were collected by means of a STOE IPDS II diffractometer. The final model included atomic positional parameters and isotropic-displacement parameters for all non-hydrogen atoms. H atoms were localized geometrically [d(C-H) = 0.93-0.97 Å, $U_{iso}(H)=1.2U_{eq}(C)$]. IR analyses were applied to in order to verify the presence of $[emim]^+$ molecules in structures of **1**, **2** и **3**. The absorption spectra were obtained in the 4000-350 cm^{-1} range using Bruker Vertex 70 IR spectrometer using KBr tablets.

The structure **1** contains one symmetrically independent β-type polyoxoanion $[Mo_8O_{26}]^{4-}$, one K cation and one [emim] molecule. The centrosymmetric $[\beta\text{-}Mo_8O_{26}]^{4-}$ unit consists of eight distorted edge-sharing $[MoO_6]$ octahedra and contains fourteen terminal ($O_{\mu1}$), six doubly bridging ($O_{\mu2}$), four triply bridging ($O_{\mu3}$), and two fivefold bridging oxygen atoms ($O_{\mu5}$). The terminal $O_{\mu1}$ atoms (O4, O5, O9, O13) of $[\beta\text{-}Mo_8O_{26}]^{4-}$ units link to K cations to form chains running along [100].

The structure **2** contains two symmetrically independent $[\beta\text{-}Mo_8O_{26}]^{4-}$ anions, one Rb cation and three [emim] molecules. Two types of $[\beta\text{-}Mo_8O_{26}]^{4-}$ units, A and B, have the same topology as units in structure **1** and similar distribution of bond distances. The A- and B-type $[\beta\text{-}Mo_8O_{26}]^{4-}$ units are connected by Rb cations to chains running along [111]. As in the structure of **1**, the Rb atoms have eightfold coordination.

The structure of **3** contains one symmetrically independent β-type polyoxoanion $[Mo_8O_{26}]^{4-}$, one Cs cation and one [emim] molecule in the structure **3**. The O atoms of $[\beta\text{-}Mo_8O_{26}]^{4-}$ units link to Cs atoms to form layers running along [010]. The Cs atoms have ninefold coordination.

In all three structures, protonated $[emim]^+$ cations are located between the inorganic $A_n[\beta\text{-}Mo_8O_{26}]$ substructures (n=1, 2), providing their linkage into a three-dimensional network through hydrogen bonding.

The structure types of the compounds studied are strongly influenced by the size of the A^+ cation. The K^+ cations with radius of 1.51 Å (Shannon, 1976) form linear

$A^+[\beta\text{-}Mo_8O_{26}]$ chains, whereas larger size of the Rb^+ cation (ri=1.61 Å) in **2** results in the appearance of two symmetrically independent polyoxoanions and the distortion of the chains. The further increase of cation size to 1.78 Å results in formation of a 2D structure, where Cs^+ cations link the $[\beta\text{-}Mo_8O_{26}]^{4-}$ units into layers. It is necessary to note that radius of metal is the leading, but not a single parameter controlling the structure type. Organic part and synthesis conditions also have considerable influence up on structure organization. Thus, the polyoxomolybdate$(4,4'\text{-}Hbpy)_2(KMo_8O_{26})$ (bpy=bipydine) has a 2D structure (Chen *et al.*, 2006), which inorganic part is topologically similar to that of **3**.

Detailed description of crystal structure and experimental details can be found in paper PII (see Included Articles).

2.1.4 Discussion

Analysis of crystal structures of five novel molybdates prepared in this work as well as of previously known members of the homologous series $A_2Mo_nO_{3n+1}$ provide some conclusions about crystal chemistry of molybdates as discussed below.

Molybdenum coordination. Octahedral coordination is the most typical for Mo^{6+}. The Mo-O bond lengths vary from 1.70 to 2.51 Å, and Δd(Mo-O) for one octahedron can be up to 0.79 Å. A distinctive feature of the $[MoO_6]^{6-}$ octahedra is the distribution of the Mo-O bonds into 3 groups: 2 short (1.70-1.76 Å), 2 medium (1.83-2.06 Å) and two long (2.13-2.51 Å) bond. Five-fold coordination for Mo^{6+} is less common. Trigonal bipyramids $[MoO_5]^{4-}$ were found in $A_2Mo_3O_{10}$ (A = K, Rb, Cs) and square pyramids in $\alpha\text{-}Cs_2Mo_4O_{13}$ and $\beta\text{-}K_2Mo_4O_{13}$. The Mo-O bond lengths vary from 1.66 to 2.39 Å. These polyhedra are also characterized by similar distribution of the bond lengths: 2 short (1.66-1.74 Å), 2 medium (1.87-1.95 Å) and one long (2.00-2.39 Å) bond are present. In four-fold coordination Mo^{6+} forms tetrahedra $[MoO_4]^{2-}$, where the bond lengths slightly vary from 1.72 to 1.87 Å.

Polyhedral connectivity. The $[MoO_6]^{6-}$ polyhedra may polymerize to each other and to the $[MoO_5]^{4-}$ polyhedra by sharing common corners and edges, whereas polymerization involving $[MoO_4]^{2-}$ proceeds along the corners only. The $[MoO_5]^{4-}$ polyhedra are found to share corners and edges with octahedra and only corners with tetrahedra. The $[MoO_4]^{2-}$ tetrahedra are either isolated or connected with other polyhedra by corner sharing. The Mo-O bond lengths strongly depend upon the type of polyhedral connectivity and, in particularly, upon the coordination number of oxygen atoms. This regularity is illustrated in **Fig. 2**, where the average values of the Mo-O bond lengths in the $[MoO_6]^{6-}$ and $[MoO_5]^{4-}$ polyhedra are drawn *versus* the coordination numbers of the oxygen atom. There is a tendency for the increasing the Mo-O bond lengths with increasing coordination number of the oxygen atoms.

Dimensional reduction. The correlation between the Mo/A ratio (A = K, Rb, Cs) and the dimensionality of the molybdate structural unit for compounds with the general formula $A_2Mo_nO_{3n+1}$ is shown in **Fig. 3**. It is obvious that the dimensionality is increasing with the increasing Mo/Cs ratio, which can be interpreted as a special case of the dimension reduction principle discussed in detail by Tulsky and Long (2001). It was reported

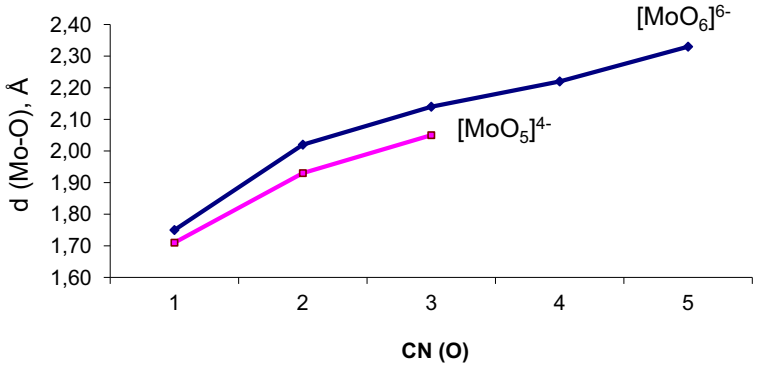

Fig. 2. Distribution of Mo-O bond lengths in $[MoO_6]^{6-}$ and $[MoO_5]^{4-}$ polyhedra in dependence on coordination number of oxygen.

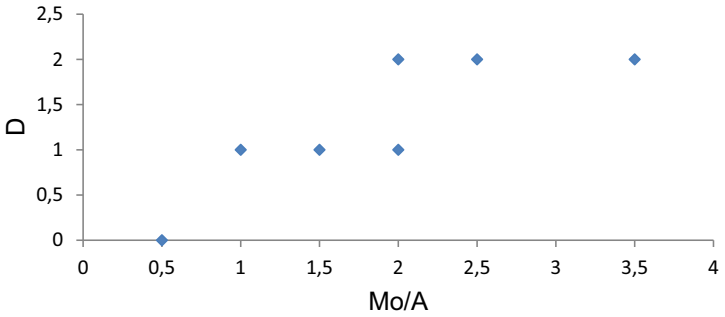

Fig. 3. Dependence of structure dimension (D) on ratio Mo/A (A = K, Rb, Cs).

that the dimension reduction is a characteristic process occurring during the introduction of ionic components into covalent structure. In general, it can be illustrated by the following reaction:

$$MX_x + nA_aX \rightarrow A_{na}MX_{x+n},$$

where A — alkali or alkaline-earth element, M — metal, X — chalcogen or halogen element. The MX_x covalent bonds in the structure of "parent" compound are becoming broken because of the introduction of *n* molecules of the A_aX ionic agent into the structure. As a consequence, a secondary compound $A_{na}MXx_{+n}$ is characterized by smaller dimensionality of the structural unit compared to the primary one. In the homologous series $A_2Mo_nO_{3n+1}$, potassium, rubidium and cesium molybdates can be represented as compounds obtained by the following reaction:

$$nMoO_3 + A_2O \rightarrow A_2Mo_nO_{3n+1},$$

where MoO_3 is the original compound with a predominantly covalent structure based on dense layers and A_2O is a dimension-reduction component. In the binary series of MoO_3-A_2O regular dimension reduction of the compound is observed with the increase of the amount of the ionic component, or the decrease of *n*.

2.2 Crystal chemical study of synthethic murataites

2.2.1 Crystal structure of murataite-3C

The sample of polyphase murataite matrix with 10 wt.% of Tb_2O_3 was provided by Institute of Geology of Ore deposites, Petrograghy, Mineralogy and Geochemistry (Moscow, Russia). Octahedral crystals of murataite were found to be zonal (**Fig. 4**). They are composed of few modifications that have different chemical composition and divided by well-defined boundaries.

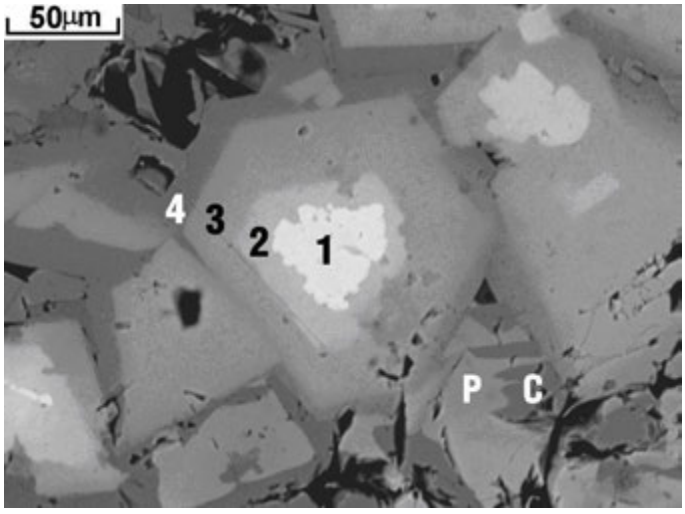

Fig. 4. SEM image of murataite matrix. 1 — zirconolite (?), 2 — *Mu*-5C (?), 3 — *Mu*-8C (?), 4 — *Mu*-3C, C — crichtonite, P — perovskite.

The X-ray diffraction data were collected using Bruker APEX II diffractometer equipped with a CCD (charge-coupled device) area detector and the STOE IPDS II diffractometer with Imaging-plate area detector. The reconstructed (110) section of reciprocal diffraction space is shown in **Fig. 5**. The strongest reflections correspond to the cubic face-centered subcell, which size is close to that of fluorite unit cell, whereas the weak reflections determine the true parameters of the murataite-3C unit cell. Observed diffuse streaks and noninteger reflections are due to the above mentioned heterogeneity of murataite grains.

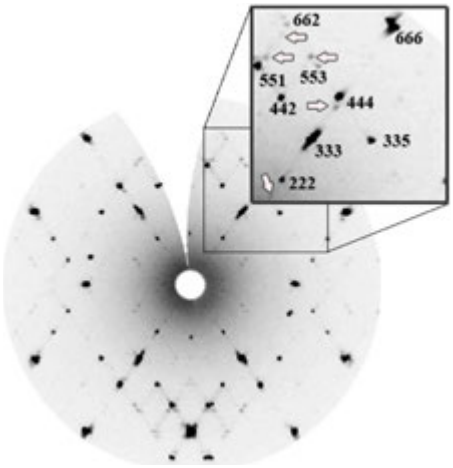

Fig. 5. The (-110) section of reciprocal diffraction space for murataite-3C. White arrows indicate positions of diffuse streaks and non-integer reflections.

The structure of synthetic murataite-3C contains five crystallographically independent cation sites. Three $Ti1O_6$ octahedra share their O3-O2 edges to form $Ti1_3O_{13}$ trimers. Four trimers are linked by sharing the O1 atoms, which results in formation of an α-Keggin $[Al^{[4]}Ti1_{12}{}^{[6]}O_{40}]$ cluster with the AlO_4 tetrahedron at its centre (**Fig. 6a, b**).

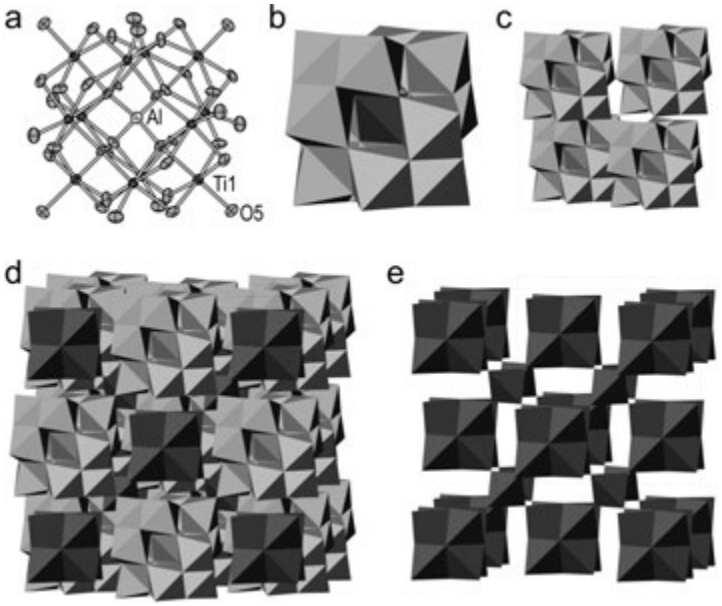

Fig. 6. Atomic structure (a) and polyhedral representation (b) of the α-Keggin cluster $[Al^{[4]}Ti1_{12}{}^{[6]}O_{40}]$ in murataite-3C; the structure viewed as an interpenetration of cation- (c) and anion-centered (e) frameworks (d).

Polymerization of Keggin units through the O5 atoms results in formation of a 3D nanoporous octahedral framework (**Fig. 6c**), where each *Ti1*O_6 octahedron shares three vertexes and two edges with five adjacent octahedra.

If each coordination polyhedron is symbolized by a node of a graph and an edge between two nodes denotes linkage of respective polyhedra, the octahedral framework can be presented as consisting of three types of structural units (**Fig. 7**): (i) a small $3^8 4^6$ cubooctahedron, which represents the α-Keggin cluster with the *Al* site in its centre; (ii) a truncated $3^4 6^4$ tetrahedron; (iii) a $4^6 6^8$ cubooctahedron, which corresponds to a large cavity with the 10 Å diameter.

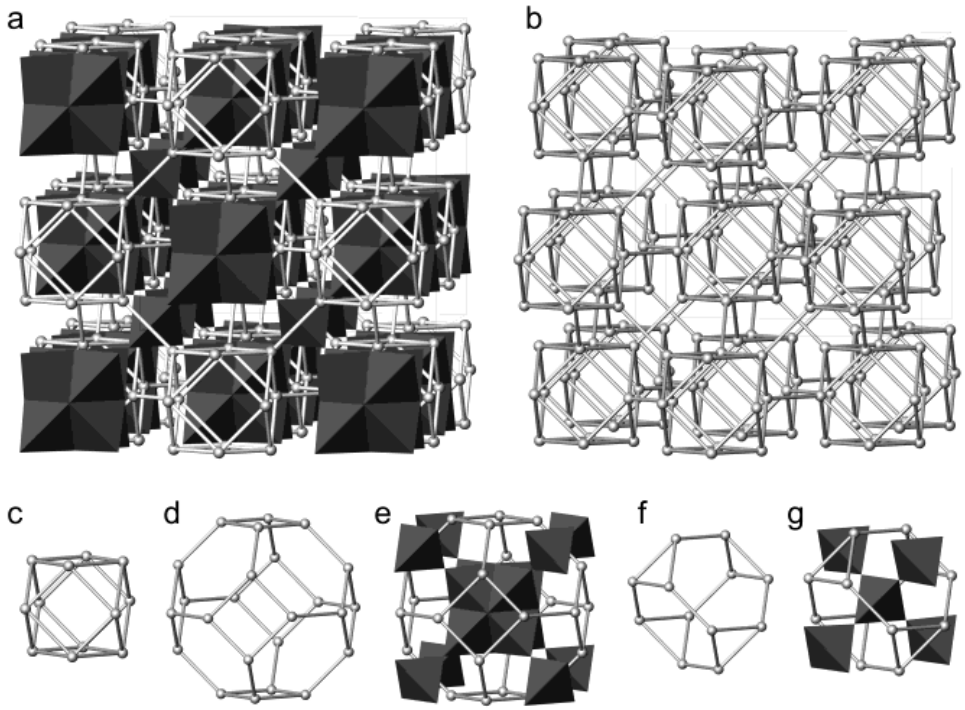

Fig. 7. Interpenentration of the anion-centered framework in murataite-3C with three-dimensional network of octahedra (each corner corresponds to an octahedral center) (a), a single network (b) and its constituents: cubooctahedron $3^8 4^6$ (c), cubooctahedron $4^6 6^8$ (d, e) truncated tetrahedron $3^4 6^4$ (f, g).

The $4^6 6^8$ cubooctahedra share their hexagonal faces with the $3^4 6^4$ truncated tetrahedra and their square faces with the $3^8 4^6$ cubooctahedra. Truncated tetrahedra and small cubooctahedra are linked through the small triangular faces (**Fig. 7**). The three structural units taken together fill the 3D space without voids and overlaps.

The structure of murataite is a 3×3×3 superstructure relative to the structure of fluorite. The ideal composition of the 3×3×3 fluorite supercell is $3^3 \times AX_2 = 27 \times AX_2 = A_{27}X_{54}$, where A and X are cations and anions, respectively. The formula of natural murataite-(Y) proposed by Ercit and Hawthorne corresponds to $^{[8]}R_6{}^{[6]}M1_{12}{}^{[5]}M2_4{}^{[4]}TX_{43}$, or $A_{23}X_{43}$,

which indicates the presence of vacancies in both cation and anion sites. The bulk formula of synthetic murataite-3C can be presented as $A_{26.76}X_{42}$. In comparison with the natural murataite, the synthetic material has noticeably less number of vacancies in the cation substructure and contains five instead of four symmetrically independent cation positions. The additional *Ca2* site (absent in the natural murataite-(Y)) is [8]-coordinated and contains Ca^{2+}, Ti^{4+}, Tb^{3+}, Mn^{2+} and Fe^{3+}. The presence of additional site increases capacity of synthetic murataite with respect to the large heavy cations such as actinides, rare earth and alkaline earth metals in comparison with the material of natural origin.

Natural murataite and its synthetic analogue are also different from the point of view of amount of anion positions. In contrast to synthetic material, which contains eight anion sites occupied by O, the natural one has seven anion sites in its structure.

The observed structural differences between synthetic and natural murataites is an inevitable consequence of their different chemical compositions. Significant amount of fluorine present in the natural samples compensates for the absence of additional cation site in natural murataite-(Y).

Detailed description of crystal structure and experimental details can be found in paper PV (see Included Articles).

2.2.2 Crystal structure model of murataite-8C

The sample of polyphase murataite matrix with 10 wt.% of Ho_2O_3 was provided by Institute of Geology of Ore deposites, Petrograghy, Mineralogy and Geochemistry (Moscow, Russia). Octahedral crystals of murataite were found to be zonal as well. The X-ray diffraction data were collected by means of Bruker APEX II diffractometer equipped with CCD (charge-coupled device) area detector and by means of a STOE IPDS II diffractometer with Image plate area detector.

In comparison with other synthetic modifications of the murataite-pyrochlore polysomatic series, murataite-8C has the crystal structure of outstanding complexity. It contains forty symmetrically independent positions of cations that is approximately one degree greater than quantity of cationic sites in the murataite-3C. Two positions are tetrahedrally coordinated, seven positions are coordinated by five oxygen atoms with formation of triangular bipyramids and fifteen positions are octahedrally coordinated. The octahedrally coordinated cations form the octahedral framework which is notable for its peculiar architecture. Three octahedra, $Ti3O_6$, $Ti4O_6$ and $Ti11O_6$, share their edges to form trimers Ti_3O_{13}. Four trimers link by corner sharing to form α-Keggin $[Ti_{12}AlO_{40}]$ cluster with tetrahedrally coordinated site *Al* in the center. It is interesting to note that α-Keggin cluster has C_{3v} symmetry in murataite-8C, whereas α-Keggin cluster observed in natural murataite and murataite-3C possesses T_d symmetry. Four α-Keggin clusters are connected by vertices O6 to form a zero-dimensional nanoscale cluster with diameter equal to 25 Å (**Fig. 8a**). This cluster can be considered as a content of murataite-3C unit-cell, therefore it was denominated as a murataite nanocluster. Murataite nanoclusters are situated at the vertices and face centers of face-centered cubic lattice so that the center of gravity of the "zero" module has the coordinates (0;0;0).

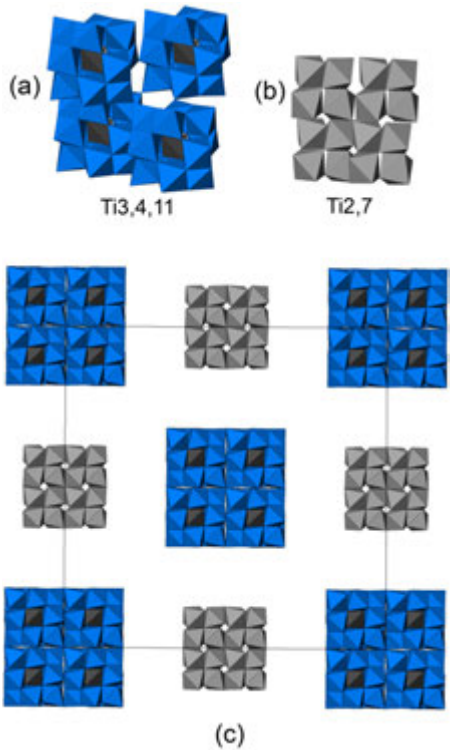

Fig. 8. Keggin-based murataite (a) and pyrochlore (b) zero-dimensional modules alternate in chessboard pattern and form the basis of murataite-8C crystal structure (c).

Another zero-dimensional built block of the murataite-8C structure is presented by pyrochlore nanocluster, which is formed by corner sharing of $Ti2O_6$ and $Ti7O_6$ octahedra (**Fig. 8b**). Pyrochlore nanocluster is about 15 Å in diameter and can be presented as a content of pyrochlore unit-cell. As well as murataite nanoclusters the pyrochlore one form the face-centered cubic lattice shifted relatively to the murataite substructure on the vector (0;0;1/2). Therefore, the murataite and pyrochlore nanoclusters, which represent the cubic unit cells of maternal structures, alternate in the three-dimensional chessboard pattern and form the basis of the murataite-8C structure (**Fig. 8c**).

The three-dimensional connectivity of murataite nanoclusters is provided by the Ti_4O_{18} tetramers composed of two $Ti1O_6$ and two $Ti8O_6$ vertices-sharing octahedra. This building unit represents the cutting out of the pyrochlore crystal structure and bears the name "pyrochlore unit" (Lord *et al.*, 2006). Murataite nanocluster is linked to twelve pyrochlore units by common oxygen vertex, each pyrochlore unit provides connection of two murataite modules. The packing of murataite nanoclusters and pyrochlore-derived building blocks in the unit cell of murataite-8C is shown in **Fig. 9**.

The octahedrally coordinated Ti6, Ti9, Ti10, Ti12, Ti13 and Ti15 sites form the octahedral transitional substructure situated between aforementioned zero-dimensional

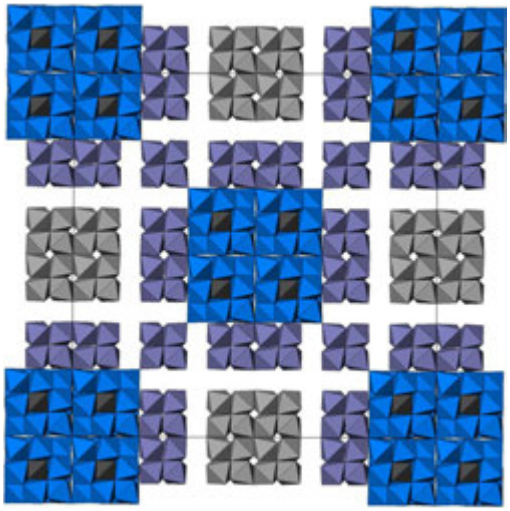

Fig. 9. The packing of murataite, pyrochlore modules and pyrochlore units in the structure of murataite-8C.

building blocks. It consists of octahedral complexes centered at the point (¼ ¼ ¼) and other equivalent points so that there are four of these complexes in the unit cell of murataite-8C (**Fig. 10a,c**). It is interesting to consider architecture of the complex from the viewpoint of nodal representation, when each coordination polyhedron is symbolized by the node of a graph and an edge between nodes denotes linkage of polyhedra (Hawthorne, 1983; Krivovichev, 2005). The nodal view of octahedral complex is presented in **Fig. 10b,d**. The transitional octahedral framework can be characterized as a combination of building units derived from the structure of murataite-3C: truncated tetrahedron $3^4 6^4$ formed by Ti6, Ti10 and Ti13 atoms and cubooctahedron $4^6 6^8$ formed by Ti12 atoms. Truncated tetrahedra $3^4 6^4$ is situated in the center of octahedral complex and share four hexagonal faces with large cubooctahedra $4^6 6^8$, which form voids with diameter about 1 nm (**Fig. 10e**). Cubooctahedral clusters are complemented by truncated pyramids $3^4 4^3 6^1$. The latter structural unit is absent in the structure of murataite-3C, whereas is observed in the structure of murataite-5C.

Thus, the octahedral structure of murataite-8C can be described as alternation of murataite and pyrochlore nanoclusters linked through the recombined murataite-3C-type substructure and additional pyrochlore units.

The structure of murataite-8C is fluorite-related with the 8×8×8 supercell. The ideal composition of the 8×8×8 fluorite supercell structure is $8^3 \times AX_2 = 512 \times AX_2 = A_{512}X_{1024}$, where A and X are cations and anions, respectively. The formula of murataite-8C derived from the structural model corresponds to the composition $A_{512}X_{823}$, which reflects significant deficit of anions with respect to the ideal fluorite structure.

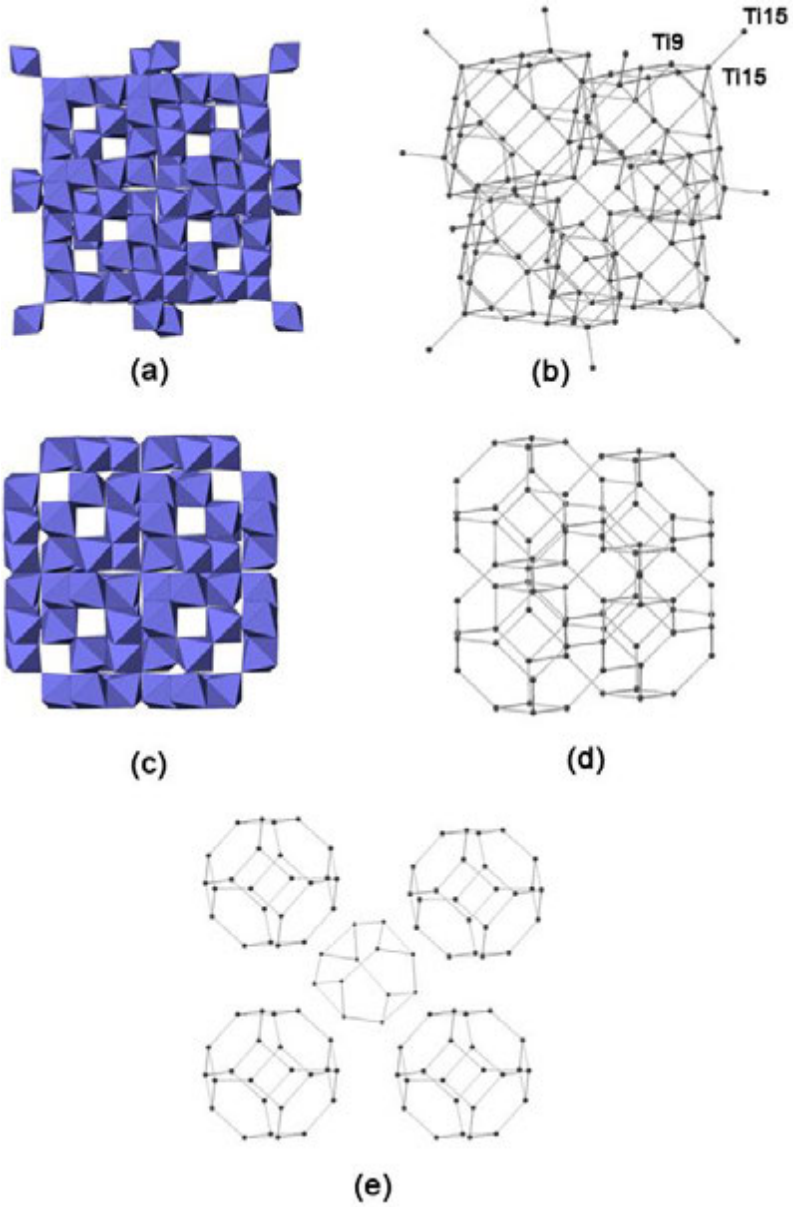

Fig. 10. The composition of transition substructure in the structure of murataite-8C: (a) octahedral cluster centered at the point (¼ ¼ ¼) and its graph representation (b); (c) the same octahedral cluster without $Ti15O_6$ and $Ti9O_6$ octahedra and its graph representation; (d) the composition of octahedral cluster as connection of four cubooctahedral voids.

2.2.3 Modular aspects of pyrochlore-murataite series

Present results of structural investigation of murataite-3C and -8C confirm the modular nature of the pyrochlore→murataite-5C→murataite-8C→murataite-3C series and elucidates its structural and chemical peculiarities. The formation of structurally diverse members is considered to be a result of combination of nanoscale zero-dimensional murataite and pyrochlore modules, which represent the structures of end series members (**Fig. 11**). Pyrochlore (*Pyr*) consists only of pyrochlore modules. In the structure of murataite-5C (*Pyr* + *Mu*), pyrochlore modules are arranged in the recombined murataite matrix. With the increase of murataite component in murataite-8C (*Pyr* + 2*Mu*), murataite modules are combined with pyrochlore modules. Murataite-3C (*Mu*) consists of murataite modules only.

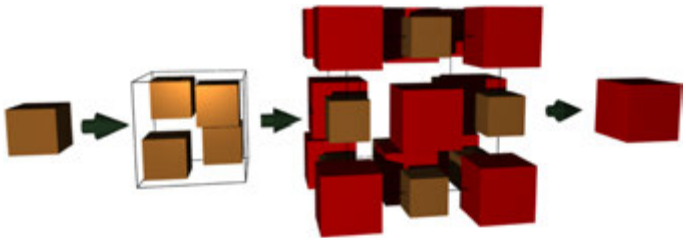

Fig. 11. Structural transition from (a) pyrochlore to (d) murataite-3C via (b) murataite-5C and (c) murataite-8C. Minor and large cubes correspond to pyrochlore and murataite modules, respectively.

Structures of pyrochlore and murataite are often considered as fluorite-related structures with the 2×2×2 and 3×3×3 supercells, respectively. Therefore, all possible module combinations can be presented as (2n+3m)×(2n+3m)×(2n+3m), where n is the number of pyrochlore modules and m is the number of murataite modules. Thereby, the combinations (0,1), (1,1), and (1,2) correspond to murataite-3C, -5C and -8C, respectively. This approach allowed Urusov and co-workers (2005, 2007) to explain the absence of murataite-4C and murataite-6C in the polysomatic series: these compounds, build upon two modules of pyrochlore and murataite, respectively, correspond to the parent structures.

The results of X-ray structural investigation of murataite modifications can account for the peculiarities of crystallization of murataite polyphase matrix and their complex chemical composition. As it was noted before, murataite matrices are characterized by zonal microstructures. The following features have been observed: central part is composed from pyrochlore, the next zone is presented by murataite-5C or/and murataite-8C and the periphery zone is composed from murataite-3C. Thereby, the crystallization process replicates the trend of polysomatic series as described above. It has been reported (Laverov *et al*., 2006) that content of actinides, rare earth elements and zirconium decreases in the polysomatic series from pyrochlore to murataite, whereas the content of titanium, aluminum and iron has a tendency to increase in the same direction. These two tendencies are connected with variations in the R/M ratio in members of polyso-

matic series, where R is a quantity of sites with eightfold and sevenfold coordination and M corresponds to quantity of sides coordinated by six, five and four oxygen atoms. The ratio R/M decreases during crystallization process, that leads to decreasing content of large atoms as Ca^{2+}, Mn^{2+}, Zr^{4+}, Gd^{3+}, Ce^{4+}, U^{4+} and Th^{4+}, which preferable occupy sites R, and simultaneous increasing of atoms Ti^{4+}, Al^{3+}, Fe^{3+} located in sites M. This zonal structure of murataite grains retards the leaching of radionuclides from the matrix and therefore enhances their stability.

2.3 Crystal structure of laachite, a new zirconolite-type mineral

The new mineral laachite was discovered by Chukanov and co-workers in a sanidinite specimen from the Laach Lake (Laacher See) volcano, Eifel region, Rheinland-Pfalz, Germany. Laachite is deep brownish-red with adamantine lustre, translucent. It forms long-prismatic crystals up to 0.02 × 0.04 × 0.5 mm, their random aggregates and twins in cavities in sanidinite (**Fig. 12**). Diffraction experiment was conducted on Bruker APEX DUO II diffractometer equipped with a CCD (charge-couple device) area detector. The structure was solved by direct methods in the space group *C*2/*c* and refined to $R_1 = 0.0312$. Pseudo-merohedral twinning was introduced into the model using matrix [-100/010/001], which improved the refinement significantly. The refined ratio between the two twin components is 0.49:0.51.

Fig. 12. Twin of laachite on sanidine. View width is 0.5 mm. Photo: Bernd Gassmann.

The crystal structure of laachite contains seven crystallographically independent cation sites. The *Ca1* and *Ca2* sites are coordinated by eight oxygen atoms each, which form distorted cubes with the average <*Ca*-O> distance of 2.465 Å. The *Zr* site is coordinated by seven oxygen atoms with the average <*Zr*-O> distance of 2.190 Å. The *Nb1*, *Nb2* and *Ti* sites are octahedrally coordinated by six oxygen atoms with the average <*M*-

O> distances of 1.953, 1.986 and 1.958 Å, respectively. The fourfold coordinated position *Fe* is splitted into two sites separated by 0.762 Å.

The crystal structure is based upon a module composed of an octahedral layer and a layer of large cations in seven- and eight-fold coordinations. The octahedral layer is built upon *Nb1*O_6, *Nb2*O_6 and *Ti*O_6 octahedra linked by corner sharing to form six- and three-membered rings (**Fig. 13a**). The Fe sites are located in the centres of six-membered rings. The second layer is composed from the *Ca*O_8 and *Zr*O_7 polyhedra. Each *Ca*O_8 polyhedron shares two opposite edges with two adjacent *Ca*O_8 polyhedra to form chains running parallel to the *a* axis. Similar chains are formed by sharing edges between the *Zr*O_7 polyhedra. Polymerization of the chains of the two types results in formation of dense layer (**Fig. 13b**). The two-layer module is formed by linkage between the octahedral layer and the layer of seven- and eightfold polyhedra (**Fig. 13c**). The modules

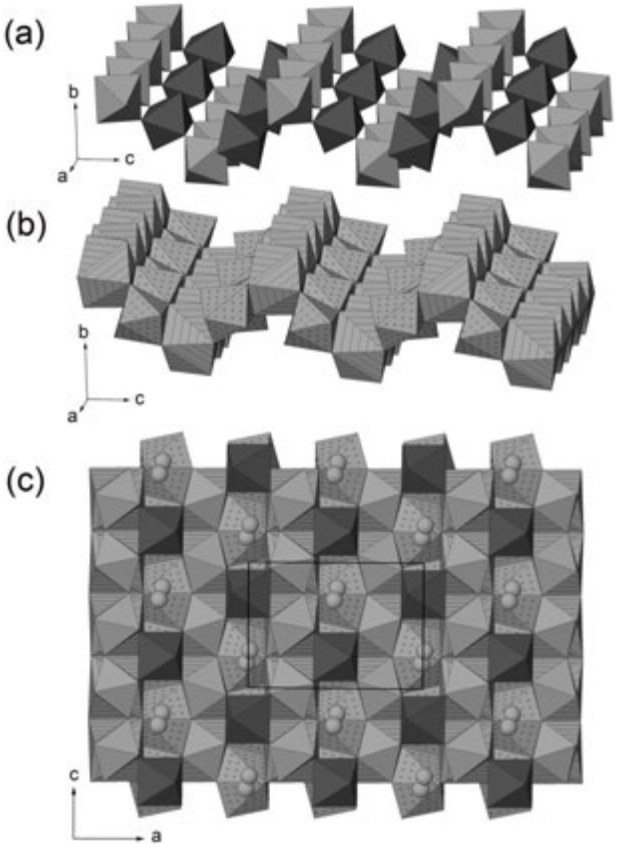

Fig. 13. Building units of the laachite crystal structure: (a) octahedral layer, (b) layer of seven- and eight-coordinated cations, (c) the module built from the octahedral and heteropolyhedral layers. Legend: *Nb*1O_6 and *Nb*2O_6 octahedra are light grey, *Ti*O_6 octahedra are dark grey, *Ca1*O_8 and *Ca2*O_8 polyhedra are light grey with lines, *Zr*O_7 polyhedra are light grey with crosses, *Fe* atoms are light grey spheres.

are stacked along the *b* axis so that adjacent modules are rotated by 180° relative to each other (**Fig. 14**).

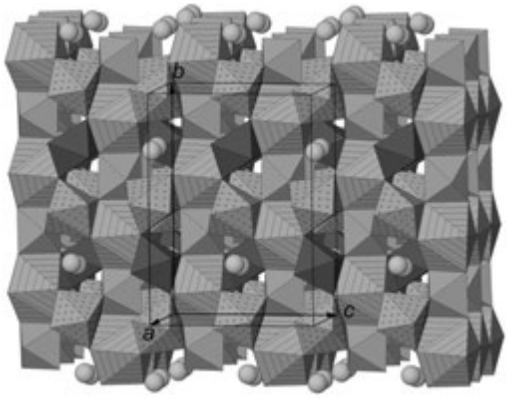

Fig. 14. The crystal structure of laachite. Legend is as in Fig. 13.

Laachite is a monoclinic analogue of orthorhombic zirconolite polytype first described by Mazzi and Munno (1983).

Conclusions

Crystal chemistry of several molybdates and titanates was investigated by means of X-ray single crystal structural analysis.

Five novel alkali molybdates were synthesized by hydrothermal (β-$Cs_2Mo_4O_{13)}$ and ionothemal method ($Cs_3(Mo_2O_7)Br$, $(emim)_3K(Mo_8O_{26})$, $(emim)_3Rb(Mo_8O_{26})$, $(emim)_2Cs_2(Mo_8O_{26})$). Ionothemal method revealed high promising perspectives for obtaining polyoxometalates. Ionic liquid 1-ethyl-3-methylimidazolium bromide, [emim] Br, used as solvent in present study, acted as structure directing agent and provided anionic part for structure construction as well as cationic. The structures of synthesized K, Rb and Cs octamolybdates showed sensitivity to the radii of alkali cation: K and Rb compounds are chain-type whereas Cs octamolybdate is layer-type. On the base of obtained structural results and previously known data some regularities of molybdates crystal chemistry were drawn. Particularly, the principle of dimensional reduction was applied for interpretation of structure variations in homologous series $Cs_2Mo_nO_{3n+1}$.

The crystal structures of murataite-3C and -8C, the members of polysomatic series pyrochlore-murataite, were solved. It gave additional evidence for previously proposed suggestion about modular nature of the series. Structure of murataite-3C was found to be close to the structure of natural murataite but has one more additional eight-coordinated site as a result of different chemical composition. Murataite-8C revealed the structure of outstanding complexity: it contains 40 cationic sites and is built on zero-dimentional

units representing unit cells of murataite and pyrochlore. The obtained structural data can explain the features of crystallization of murataite matrixes and zonal distributions of actinide elements within.

Finally, new zirconolite-related mineral laachite, $(Ca,Mn)_2(Zr,Mn)_2Nb_2TiFeO_{14,}$ was structurally characterized. It was found to be monoclinic analogue of previously known polytype zirconolite-3O. The main feature is the dominancy Nb over Ti in octahedrally coordinated sites.

The results of present study contribute to the fundamental knowledge of crystal chemistry of molybdates and titanates as well as have direct practical application. For instance, murataite matrixes are already probationary used for radioactive waste immobilization in Dimitrovgrad facility, Russia.

REFERENCES

Adams J. W., Botinelly T., Sharp W. N., Robinson K. Murataite, a new complex oxide from El Paso Country, Colorado // Am. Mineral. 1974. Vol. 59. P. 172-176.

Bayliss P., Mazzi F., Munno T. J., White R. Mineral nomenclature: zirconolite // Mineral. Mag. 1989. Vol. 53. P. 565–569.

Becher, H. J., Fenske, D. Crystal and Anion Structure of the Double Salt Potassium Bromide-Potassium Dimolybdate // J. Chem. Res. (S). 1978. P. 167.

Chen Y., Shen X., Zhang H., Huang C., Cao Y., Sun R. The structure and two-dimensional correlation infrared spectroscopy study of a new 2D polyoxomolybdate complex containing β-octamolybdate linked up by potassium ions: (4, 4'-Hbpy)$_2$($K_2Mo_8O_{26}$) // Vib. Spectrosc. 2006. Vol. 40. P. 142.

Choppin G., Liljenzin J., Rydberg J. Radiochemistry and nuclear Chemistry. Butterworth-Heinemann. 2001. 720 p.

Cordfunke E. H. P., Konings R. J. M. Thermochemical data for reactor materials and fission products. 1990. P. 150–155.

Energy, electricity and nuclear power estimates for the period up to 2050 // International Atomic Energy Agency. Reference Data Series. Vienna, 2011. No1. P. 60.

Ercit T. S., Hawthorne F. C. Murataite, a UB_{12} derivative structure with condensed Keggin molecules // Can. Mineral. 1995. Vol. 33. P. 1223–1229.

Fallon G. D., Gatehouse B. M. The crystal structure of a complex cerium(III) molybdate containing a dimolybdate chain, $Ce_2(MoO_4)_2(Mo_2O_7)$ // J. Solid State Chem. 1982. Vol. 44. P. 156–161.

Gatehouse B. M., Leverett P. Crystal structure of potassium tetramolybdate, $K_2Mo_4O_{13}$, and its relationship to the structures of other univalent metal // J. Chem. Soc. (A). 1971. P. 2107–2112.

Hawthorne F. C. Graphical enumeration of polyhedral clusters // Acta Cryst. 1983. V. A39. P. 724–736.

Ishii T., Mizuno T. Thermal conductivity of cesium molybadate Cs_2MoO_4 // J. Nucl. Mater. 1996. Vol. 231. P. 242–244.

Krivovichev S. V. Topology of microporous structures // Rev. Mineral. Geochem. 2005. V. 57. P. 17–68.

Krivovichev S. V., Yudintsev S. V., Stefanovsky S. V., Organova N. I. Karimova O. V., Urusov V. S. Murataite-pyrochlore series: a family of complex oxides with nanoscale pyrochlore clusters // Angew. Chem. Int. Ed. 2010. V. 49. P. 9982–9984.

Laverov N. P., Sobolev I. A., Stefanovsky S. V., Yudinzev S. V., Omel'yanenko B. I., Nikonov B. S. Synthetic murataite: a new mineral for actinide immobilization // Dokl. Akad. Nauk. 1998_1. Vol. 362. No. 5. P. 670–672. [Dokl. Earth Sci. (Engl.Transl.) 1998_1. Vol. 363. P. 1104–1106].

Laverov N. P., Gorshkov A. I., Yudinzev S. V., Sivtsov A. V., Lapina M. I. New structural species of the synthetic murataite // Dokl. Akad. Nauk. 1998_2. Vol. 363. No. 4. P. 540–543. [Dokl. Earth Sci. (Engl. Transl.) 1998_2. Vol. 363A. P. 1272–1274].

Laverov N. P., Yudintsev S. V., Omel'yanenko B. I., Nikonov B. S. Murataite ceramics for the immobilization of actinides // Geol. Rudn. Mestorozhd. 1999. Vol. 41. No. 2. P. 99–108 [Geol. Ore Deposits (Engl. Transl.). 1999. Vol. 41. No. 2. P. 85–93].

Laverov N. P., Yudintsev S. V., Stefanovsky S. V., Jang Y. N. New actinide matrix with pyrochlore structure // Dokl. Akad. Nauk. 2001. Vol. 381. No. 3. P. 399–402 [Dokl. Earth Sci. (Engl. Transl.). 2001. Vol. 381A. No. 9. P. 1053–1056].

Laverov N. P., Yudintsev S. V., Yudintseva T. S., Stefanovsky S. V., Ewing R. C., Lian J., Utsunomiya S., Wang L. M. Effect of radiation on properties of confinement matrices for immobilization of actinide-bearing wastes // *Geol. Rudn. Mestorozhd.* 2003. Vol. 45. No. 6. P. 483–513 [*Geol. Ore Deposits* (Engl. Transl.). 2003. Vol. 45. No. 6. P. 423–451].

Laverov N. P., Yudintsev S. V., Stefanovsky S. V., Omel'yanenko B. I., Nikonov B. S. Murataite as a universal matrix for immobilization of actinides // Geol. Rudn. Mestorozhd. 2006. Vol. 48. P. 387–409 [Geol. Ore Deposits (Engl. Transl.). 2006. Vol. 48. P. 335–356].

Lian J., Wang L. M., Ewing R. C., Yudintsev S. V., Stefanovsky S. V. Ion beam-induced amorphization and order-disorder transitions in the murataite structure // J. Appl. Phys. 2005. V. 97. № 113536.

Lord E. A., Mackay A. L., Ranganathan S. // New geometries for new materials. Cambridge University Press, 2006.

Mazzi F., Munno R. Calciobetafite (new mineral of the pyrochlore group) and related minerals from Campi Flegrei, Italy; crystal structures of polymignite and zirkelite: comparison with pyrochlore and zirconolite // Am. Mineral. 1983. Vol. 68. P. 262–276.

Minato K., Takano M., Fukuda K., Sato S., Ohashi H. Thermal expansion and thermal conductivity of cesium molybdate // J. Alloys Compd. 1997. Vol. 255. P. 18–23.

Morgan P. E. D., Ryerson F. J. A "new" crystal compound // J. Mater. Science Letters. 1982. Vol. 1. № 8. P. 351–352.

Portnov A. M., Dubakina L. S., Krivokoneva G. K. Murataite in the forecasted assemblage with landauite // *Dokl. Akad. Nauk SSSR.* 1981. Vol. 261. No. 3. P. 741–744.

Ringwood A. E. Disposal of high-level nuclear wastes: a geological perspective // Mineralogical Magazine. 1985. V. 49. P. 159–176.

Shannon R. D. Revised Effective ionic radii and systematic studies of international distances in halides and chalcogenides // Acta Cryst. 1976. Vol. A32. P. 751–767.

Sheldrick G. M. // SHELX-97: Program for the Solution and Refinement of Crystal Structures. Univ. of Gottingen. 1990.

Short R. J., Hand R. J., Hyatt N. C., Mąbus G. Environment and oxidation state of molybdenum in simulated high nuclear waste glass composition // J. Nuclear Materials. 2005. Vol. 340. P. 179–186.

Stadnicka K., Haber J., Kozłowski R. The crystal structure of magnesium dimolybdate // Acta Cryst. 1977. Vol. B33. P. 3859–3862.

Tulsky E. G., Long J. R. Dimentional reduction: a practical formalism for manipulating solid structures // Chem. Mater. 2001. Vol. 12. P. 1149–1166.

Urusov V. S., Organova N. I., Karimova O. V., Yudintsev S. V., Stefanovsky S. V. Synthetic "murataites" as modular members of a pyrochlore-murataite polysomatic series // Dokl. Akad. Nauk. 2005. Vol. 401, P. 226–232 [Dokl. Earth Sci. (Engl. Transl.). 2005. Vol. 401. P. 319–325].

Urusov V. S., Organova,N. I., Karimova O. V., Yudintsev S. V., Ewing R. C. A modular model of the crystal structure of the pyrochlore–murataite polysomatic series // *Kristallografiya*. 2007. Vol. 52. P. 41–49 [*Crystallogr. Rep.* (Engl. Transl.), 2007. Vol. 52. P. 37–46].

Yudintsev S. V., Stefanovsky S. V., Nikonov B. S., Maslakov K. I., Ptashkin A. G. Structural characterization of Pu-bearing murataite ceramic // J. Alloys Compd. 2007. V. 444–445. P. 606–609.